Pediatric Pathologies that have Leukocoria as Presenting Sign: the Podium

Paolo Galluzzi; Sara Leonini; Alfonso Cerase; Alessandro Rossi

Neuroimaging and Neurointerventional Unit (NINT), Azienda Ospedaliera e Universitaria Senese, Siena, Italy

Abstract

Leukocoria is a condition in which the normal red reflex of the retina is replaced by a yellowish or grayish white color. Retinoblastoma is the most common cause of leuko-coria in the pediatric age, followed by persistent fetal vasculature and Coats' disease. Clinical and imaging signs and differential diagnosis features of these pathologies are evaluated.

Introduction

Leukocoria or cat's eye is a white, pink-white, or yellow-white reflex resulting from any white or light-colored intraocular retrolental abnormality (mass, membrane, retinal detachment, or retinal storage disease), that reflects incident light back through the pupil towards the observer (Fig. 1). Leukocoria is the most common presenting sign of retinoblastoma (RB), the highly malignant primary retinal cancer which is the most common intraocular tumor of childhood. Intraocular lesions presenting with leukocoria are usually diagnosed at ophthalmoscopy, however the detection and clinical differentiation between RB and other benign simulating lesions (so-called 'pseudoretinoblastoma') may be difficult [1-6]. Imaging therefore may play a pivotal role in the differential diagnosis.

In addition to RB, which is the most frequent cause of leukocoria in children, the second and third most common ones are persistent fetal vasculature (PFV) and Coats' disease (CD), respectively.

Methods

The routine imaging protocol of children[1] with leukocoria in our institution takes about one hour. Our patients with leukocoria are studied in a 1.5T system (MAGNETOM Avanto, Siemens Healthcare, Erlangen, Germany) with a head coil and a surface coil for each eye (diameter 4 cm); our protocol includes pre-contrast T1, T2-weighted (transaxial) thin-slice (≤ 2 mm) imaging.

The measured voxel of the T1w sequences acquired with the orbit coils are 0.43 x 0.3 x 2 mm (TR 312 ms, TE 15 ms, FOV 75, base/phase resolution 256/80). Turbo spin echo (TSE) 3D T2-weighted images (TR 750 ms, TE 112 ms, FOV 170, base/phase resolution 256/100, slice thickness 0.7 mm) and have 0.7 x 0.7 x 0.7 isotropic voxels. Gradient-echo (GRE) 3D T2-weighted steady-state free precession sequences (TR 47 ms, TE 20 ms, FOV 180, base/phase resolution 384/93, slice thickness 1 mm) have voxels of 0.6 x 0.5 x 1 mm. Recently, GRE 3D T2-weighted imaging has been replaced by susceptibility-weighted imaging with the same slice thickness and with voxels of 0.7 x 0.5 x 1 mm (TR 46, TE 38, FOV 100, base/phase resolution 192/75). The study of the orbits also includes diffusion-weighted sequences (DWI) (TR 3200, TE 100, FOV 100, base/phase resolution 192/100, voxel size 1.2 x 1.2 x 2.6 mm), and post-contrast T1-weighted (sagittal oblique and transaxial, gadoteric acid (Dotarem, Guerbet, France)) without fat-saturation. 1 mm-thick fat-suppressed post-contrast T1-weighted Volumetric Interpolated Breathhold Examination (VIBE) images (TR 9.14, TE 4.39, FOV 75 mm, 2 averages, base/phase resolution 256/75, voxel size 0.4 x 0.3 x 1 mm) are also used to obtain volumetric imaging and to better evaluate orbital spread of the tumor. Dynamic Contrast Enhanced (DCE) images are also performed to evaluate contrast enhancement degree in early, medium and late phases. Imaging of the head includes pre-contrast sagittal T1 and T2-weighted, transaxial PD and T2-weighted (slice thickness ≤ 4 mm) and post-contrast 3D magnetization prepared rapid gradient echo (MPRAGE) sequences (TR 2070 ms,

[1] MR scanning has not been established as safe for imaging fetuses and infants under two years of age. The responsible physician must evaluate the benefit of the MRI examination in comparison to other imaging procedures.

1 Left eye leukocoria.

TE 3.52 ms, ST 1 mm, FOV 109 mm, base/phase resolution 384/75) of the whole brain, performed using the standard head coil.

All children are deeply sedated for the examinations to reduce motion artifacts.

Retinoblastoma

RB is a highly malignant primary retinal tumor arising from neuroectodermal cells (nuclear layer of the retina). Though rare, it is the most common intraocular tumor of childhood. The incidence of RB varies from 1 : 17,000 to 1 : 24,000 live births [7]. Most patients present before four years of age (mean age 24 months for unilateral and 12 months for bilateral cases) [8], but 30 to 40% of patients will have a germline mutation in the RB1 gene and present at an earlier age with multifocal, bilateral disease [9]. Patients with the genetic form of RB are at an increased risk for developing primary intracranial neuroectodermal tumors in the pineal or suprasellar region usually with a dismal prognosis, a condition termed 'trilateral retinoblastoma' [10-13].

RB was classified into five groups by Reese and Ellsworth [14] to provide a prognosis for local cure and vision of eyes treated with external beam radiotherapy (EBT). More recently, an international classification for intraocular RB (ABC) has been created for the purpose of clinical trials using chemotherapy [15] (Tables 1, 2).

The growth pattern of RB may be endophytic, from the retina into the vitreous, exophytic into the subretinal space and mixed, whereas the diffuse pattern with flat infiltration along the retina (so-called diffuse infiltrative retinoblastoma or DIRB) is uncommon [16].

It is not uncommon to observe an RB growing in an eye that is smaller than normal, but its occurrence in micro-ophthalmic eyes is extremely rare, with the exception of cases with a phthisis bulbi.

Diagnosis of RB is usually made by ophthalmoscopy (under general anesthesia). The more usual opthtalmoscopic appearance of RB is one or more pink-whitish tumor/s projecting

Table 1: Reese-Ellsworth Classification

Group 1 (very favorable for saving [or preserving] the eye)
1A: one tumor, smaller than 4 disc diameters (DD), at or behind the equator
1B: multiple tumors smaller than 4 DD, all at or behind the equator
Group 2 (favorable for saving [or preserving] the eye)
2A: one tumor, 4 to 10 DD, at or behind the equator
2B: multiple tumors, with at least one 4 to 10 DD, and all at or behind the equator
Group 3 (doubtful for saving [or preserving] the eye)
3A: any tumor in front of the equator
3B: one tumor, larger than 10 DD, behind the equator
Group 4 (unfavorable for saving [or preserving] the eye)
4A: multiple tumors, some larger than 10 DD
4B: any tumor extending anteriorly (toward the front of the eye) to the ora serrata (front edge of the retina)
Group 5 (very unfavorable for saving [or preserving] the eye)
5A: tumors involving more than half of the retina
5B: vitreous seeding (spread of tumors into the gelatinous material that fills the eye)

Table 2: International Classification of Retinoblastoma

Group	Subgroup	Quick reference	Specific features
A	A	Small tumor	Retinoblastoma < 3 mm in size
B	B	Larger tumor	Retinoblastoma > 3 mm in size
		Macula	Macular retinoblastoma location (< 3 mm to foveola)
		Juxtapapillary	Juxtapapillary retinoblastoma location (< 1.5 mm to disc)
		Subretinal fluid	Clear subretinal fluid > 3 mm from margin
C		Focal seeds	Retinoblastoma with
	C1		Subretinal seeds < 3 mm from retinoblastoma
	C2		Vitreous seeds < 3 mm from retinoblastoma
	C3		Both subretinal and vitreous seeds > 3 mm from retinoblastoma
D		Diffuse seeds	Retinoblastoma with
	D1		Subretinal seeds > 3 mm from retinoblastoma
	D2		Vitreous seeds > 3 mm from retinoblastoma
	D3		Both subretinal and vitreous seeds > 3 mm from retinoblastoma
E	E	Extensive retinoblastoma	Extensive retinoblastoma occupying > 50% globe or Neovascular glaucoma
			Opaque media from hemorrhage in anterior chamber, vitreous or subretinal space
			Invasion of postlaminar optic nerve, choroid (2 mm), sclera, orbit, anterior chamber

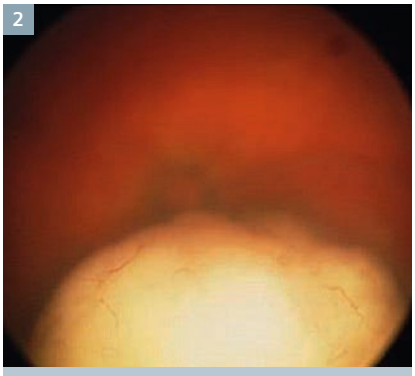

2 Whitish intraocular mass at ophthalmoscopy.

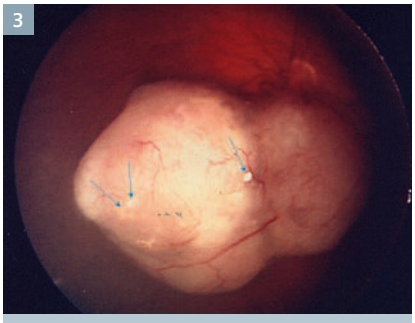

3 Superficial calcifications (arrows).

4 Feeder vessels in a large retinoblastoma.

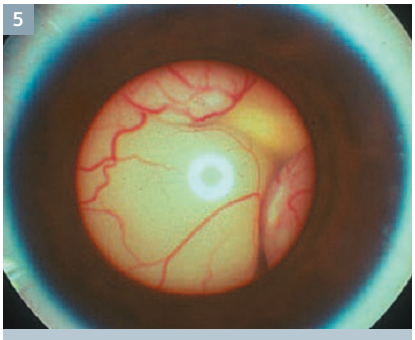

5 Bullous total retinal detachment.

into the vitreous (Fig. 2); calcifications and hypertrophic feeder vessels are more frequently encountered in medium-large size masses (Figs. 3, 4).

Intratumoral calcification and/or tumor seeding give additional support to an ophthalmoscopic diagnosis of RB. Tumoral mass development may result in retinal detachment (Fig. 5), choroidal and/or optic nerve infiltration, ciliary body invasion and anterior segment extension.

Solitary or multiple intraocular masses, often with calcification, whether or not associated with retinal detachment and vitreous seeding are readily visible by ultrasound (US). Particularly, at A-scan US the tumor shows high internal reflectivity and rapid attenuation of the normal orbital pattern, whilst B-scan US shows a round or irregular mass with high reflective echoes and a variable degree of calcification (i.e. shadowing) (Fig. 6). Ultrasound biomicroscopy (UBM) allows *in vivo* analysis of the anterior segment of the eye at microscopic resolution, providing a sensitive and reproducible visualization of the anterior retina, ciliary region, and anterior segment allowing a better staging of the advanced disease process, anterior to the ora serrata [17].

Both ophthalmoscopy and US may be limited by the presence of complex intraocular interfaces when vitreous opacities, subretinal fluid, and retinal detachment are present, have very limited ability to evaluate tumor extension into the optic nerve and may not detect the ocular wall and the extraocular space compared to MR imaging [18-22].

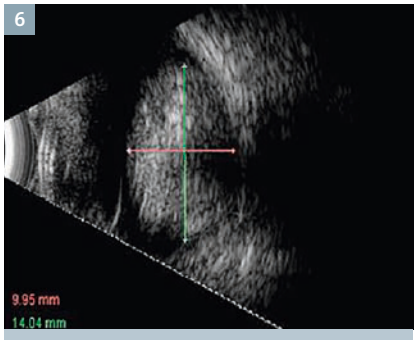

6 Large hyperechogenic mass with shadowing.

With 3D US, extrascleral extension and optic nerve invasion can be scrutinized with unique previously unavailable oblique and coronal sections, but shadowing can consistently reduce the reliability of this technique [23].

Ocular coherence tomography (OCT) is a valuable tool for assessment of cross-sectional retinal anatomy, with axial resolution to approximately 10 mm. Deeper tissues such as the choroid and sclera are imaged. OCT scans have also been used favorably during the management of RB [24-26]. On OCT, RB shows an optically dense appearance. Intralesional calcification can cause higher internal reflectivity (backscattering) and denser shadowing. There is abrupt transition of the normal retinal architecture to the retinal mass. OCT is also a useful test in monitoring reasons for visual loss following treatment of RB [24]. However, with the current clinical OCT platforms, it is very difficult to successfully image small children with RB without sedation.

Guidelines from European Retinoblastoma Imaging Collaboration (ERIC) to standardize MRI of the eye have been recently published [27].

MRI demonstrates lesions that are slightly hyperintense to vitreous on T1-weighted sequences and hypointense to vitreous on T2-weighted sequences (Figs. 7-8), a feature that can be used to differentiate RB from PFV and CD that usually produce hyperintense abnormalities in both T1 and T2w images. Calcification is the most important differentiating feature of RB. The vast majority of RB appear nodular with calcifications. Only a few pathologic conditions other than RB show calcium deposits in extremely young children. These include microphthalmos with and without colobomatous cysts, choristoma, and cytomegalovirus (CMV) endophthalmitis [28-29]. In children older than three years of age, several additional lesions, such as astrocytoma of the retina, retinopathy of prematurity (ROP), toxocariasis, medulloepithelioma, and optic nerve drusen, may have calcifications, thus mimicking the appearance of RB. The common CT appearance of RB is that of a mild to moderate hyperdense lesion, very frequently

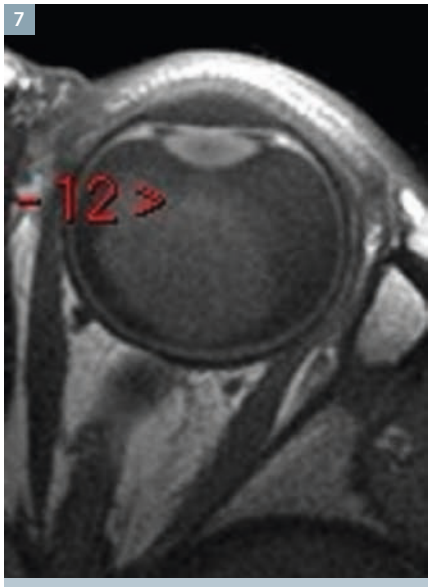

7 The mass is slightly hyperintense on T1-weighted image.

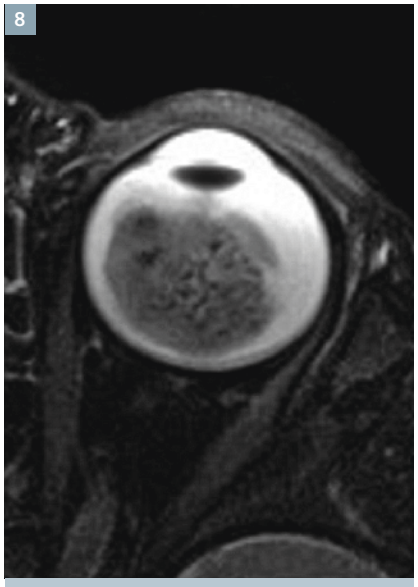

8 The mass is hypointense on T2-weighted image.

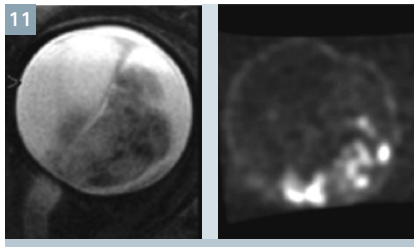

11 Correspondence between signal voids at MR (left side) and hyperdensities at *ex vivo* CT scan.

12 Susceptibility-weighted image (SWI) ameliorates the documentation of signal voids consistent with calcifications.

with calcifications and moderate to marked enhancement after contrast administration (Fig. 9). Our protocol does not include CT for assessment of intraocular tumors to avoid exposure of patients to ionizing radiation. A high-resolution gradient-echo T2-weighted sequence showed promising results regarding detection of calcifications [30] (Fig. 10). Galluzzi et al. [30] showed that when data from ophthalmoscopy, US and MRI are put together, no calcifications detected on CT were missed. More recently, signal-intensity voids indicating calcification on gradient-echo T2-weighted sequences were compared with *ex vivo* high-resolution CT: all calcifications visible on high-resolution CT could be matched with signal-intensity voids on MRI [31] (Fig. 11). Sensitivity of susceptibility-weighted imaging for detecting intratumoral calcifications is under evaluation (Fig. 12).

The tumor variably enhances with intravenous gadolinium contrast material (Fig. 13).

Diffuse infiltrating RB (DIRB) is a rare form of RB, generally presenting at a more advanced age than the typical unilateral form, and occurs more frequently in boys. It is consistently reported as being unilateral and sporadic [32-34]. Pseudo-inflammation is a common presenting sign (24% versus only 6% in the classic

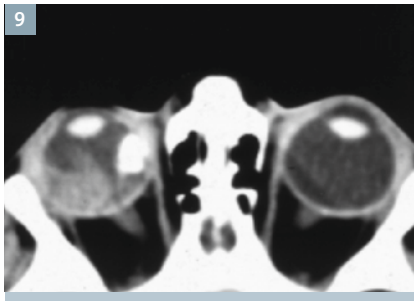

9 Contrast-enhanced CT scan showing enhancement of a partially calcified right eye mass.

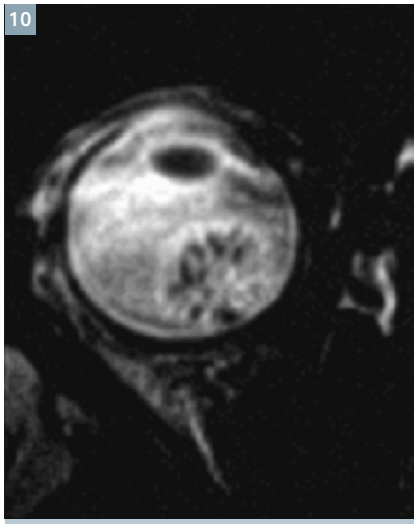

10 Intratumoral signal voids on gradient-echo 3D T2*-weighted image, consistent with calcifications.

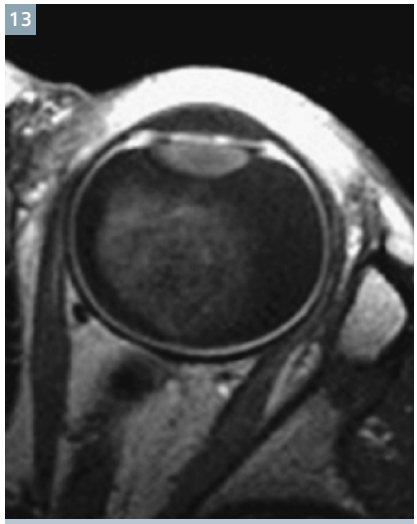

13 T1-weighted image after contrast administration showing moderate enhancement of the mass.

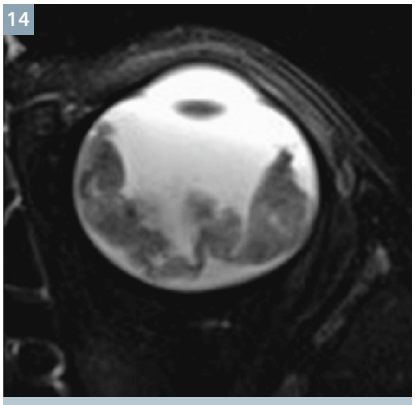

14 T2-weighted image of a diffuse infiltrating retinoblastoma (DIRB).

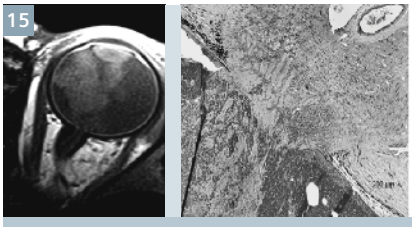

15 Histologically confirmed prelaminar optic nerve infiltration with interruption of choroido-retinal enhancement line at optic disc level.

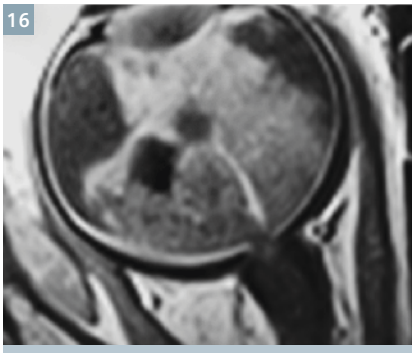

16 T1-weighted contrast-enhanced image showing retrolaminar optic nerve infiltration.

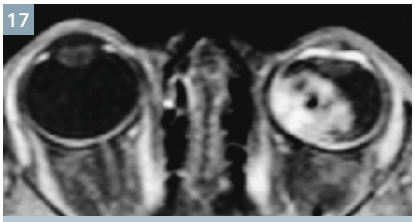

17 T1-weighted contrast-enhanced image showing abnormal anterior segment enhancement of the left eye.

form), whereas leukocoria is relatively rare (24% versus 63% in the classic form), such as calcifications (14.3% of cases at histology) [33]. On clinical examination, pseudohypopyon is a suggestive sign, observed in 59% of cases [32]. On MR images it appears as an exophytic mass with relatively high signal intensity on T1-weighted sequences, low signal intensity on T2-weighted sequences, and moderate contrast enhancement. The detached retinal leaflets appeared to be diffusely thickened, irregular, and locally nodular, with possible contrast enhancement [32-34] (Fig. 14).

RB behaves aggressively, employing several modes of dissemination, but patients have a very high life expectancy, if the tumor is diagnosed early; the options for eye-preserving therapy have significantly improved over recent years [35-38].

As a consequence, more children are treated without histopathological confirmation and, what is more important, without assessment of risk factors for disease dissemination and prognosis.

Invasion of the optic nerve in RB is quite common. From there, neoplastic cells may then breach the pia to reach the subarachnoid space or spread into the intracranial optic pathways. Interruption of the normal linear enhancement at the optic nerve disk (choroidoretinal complex) supports a suggestion of prelaminar optic nerve invasion [39-41] (Fig. 15). Postlaminar nerve invasion is the presence of abnormal contrast-enhancement (enhancement ≥ 2 mm in diameter) in the distal nerve [42] (Fig. 16); when evaluating optic nerve enhancement we must pay attention to the presence of elevated intraocular pressure (IOP), that could lead to a false bulging of the tumor in the optic nerve head. The accuracy of MRI in detecting optic nerve invasion has been assessed in several studies [8, 27, 40, 42, 43, 44]. In a recent meta-analysis, De Jong et al. [45] reported the sensitivity and specificity of conventional MRI in detecting postlaminar nerve invasion to be 59% (95% CI, 37-78%) and 94% (95% CI, 84-98%), respectively.

Recent publications have suggested a limited correlation of MRI with histopathology and there is little agreement among radiologists' interpretations [46-49]. However, these authors used standard-resolution MRI with head coils; the use of surface coils is currently recommended [43, 44]. High-resolution MRI with surface coils excludes advanced optic nerve invasion with high negative predictive value and is recommended for the appropriate selection of RB patients eligible for primary enucleation. However, it cannot substitute for pathology in differentiating the first degrees of nerve invasion [50].

Postlaminar optic nerve or optic nerve meningeal sheath invasion should raise suspicion of leptomeningeal metastases.

Invasion of the choroid and sclera may occur with subsequent extension into the orbit, conjunctiva, or eyelid. The risk of distant metastasis increases markedly with extraocular extension.

Discontinuity of the normal choroidal enhancement is the leading criterion for its infiltration. Massive choroidal invasion usually presents as focal choroidal thickening. Protrusion of enhancing tissue through the thickened choroid into the (low signal-intensity) sclera or beyond is a sign of scleral invasion or extraocular extension, respectively [40].

Anterior eye segment enhancement frequently occurs in RB and is usually a sign of iris angiogenesis, caused by the hyper-secretion of vascular endothelial growth factor (VEGF) in tumor growth-induced ischemia [51, 52] (Fig. 17). Tumor invasion into the anterior eye segment is an infrequent finding [40].

Vitreous seeding can be shown by MRI only if the tumoral flocculus are large enough to be detected and dedicated sequences are performed (Fig. 18).

DWI has been widely used in evaluation of orbital tumors in adults and children. In our protocol, DWI images of the eye(s) and the optic nerve(s) were acquired in the three orthogonal directions with b-factors of 0, 500, and 1000 mm^2/s and apparent diffusion coefficient (ADC) maps were automati-

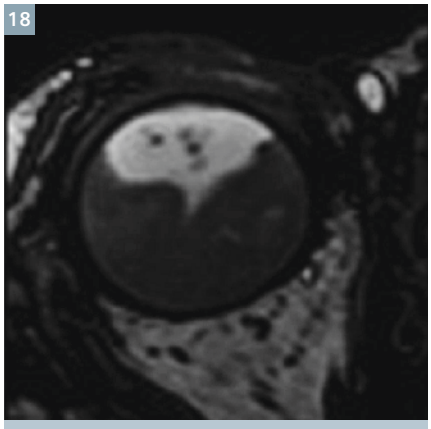

18 T2-weighted 3D image showing small hypointense floccules of vitreal seeding.

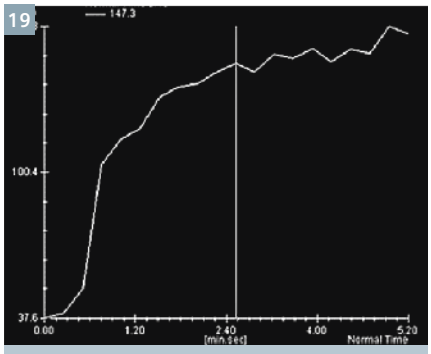

19 Dynamic curve showing early enhancement with progressive growth.

cally generated. Preliminary results in RB consistently demonstrate low ADC within the tumor and a correlation between its value and prognostic parameters [53] (Fig. 19): actually, findings such as poorly differentiated or undifferentiated tumor, bilaterality, large size tumors, and optic nerve invasion are usually associated with a trend for lower ADC [54, 55].

There has been recent discussion of the potential for dynamic contrast-enhanced (DCE) MRI to non-invasively assess tumor angiogenesis and necrosis in RB concluding that the early phase of the DCE time curve positively correlates with microvascular density, while the presence of late enhancement correlates with necrosis [56] (Fig. 20).

Brain MRI can detect trilateral RB (i.e. PNET located mainly in the pineal gland, or rarely in the suprasellar area), leptomeningeal spread and

20 Restricted diffusion within the tumor.

congenital brain malformations (mainly in patients with 13q-deletion syndrome) [57, 58].

Persistent fetal vasculature (Persistent hyperplastic primary vitreous)

PFV (previously named persistent hyperplastic primary vitreous) is the second most common cause of leukocoria. It is a congenital, non-hereditary, failure of the embryonic primary vitreous to regress, resulting in continued proliferation and formation of a retrolental mass with cataract in the anterior segment. The primary vitreous is formed during the first month of development, extends from the posterior lens to the retina and contains branches of the hyaloid artery. The hyaloid blood system consists primarily of the hyaloid artery, a branch of the ophthalmic artery, and by the vasa hyaloidea propria. The hyaloid artery begins to regress during the formation of the avascular secondary vitreous at nine weeks. By the third month, the secondary vitreous, which ultimately forms the adult vitreous, fills most of the developing vitreous cavity. The primary vitreous becomes condensed into a narrow band (Cloquet's canal), running from the optic disc to the posterior aspect of the lens.

Usually, the primitive hyaloid system regresses completely: the posterior portion of the arterial system typically regresses at seven months of life, whilst the anterior one regresses at eight months of life. When the primitive mesenchymal tissue persists and continues to proliferate, a retrolental mass is formed. Commonly, patients have a combination of the anterior and posterior types of PFV. In the anterior type, findings include a shallow anterior chamber, elongated ciliary processes, enlarged iris vessels, cataracts, early onset glaucoma, and intralenticular hemorrhages (Fig. 21). There is also commonly degeneration of the lens fibers; this may manifest as an abnormal lental morphology at imaging and ultimately may lead to development of a cataract [59]. In the posterior type, findings include the classic retrolental fibrovascular mass, vitreous membrane, a remnant of the Cloquet canal, which carries the hyaloid artery, optic disc dysplasia, and a clear lens [60]. The retrolental mass may hinder the proper development of the retina and lead to variable degrees of microphthalmia. In older patients, calcification or even ossification of the lens may be observed [61].

PVF is unilateral in between 90%-98% of cases [61-63].

Rare bilateral cases of similar findings have been reported in the past in association with Norrie disease, Warburg syndrome, and other neurologic and systemic anomalies [61]. However, bilateral PFV may represent a separate clinical entity, with a unique underlying mechanism and several bilateral PFV have been recently described [64-67].

Retinal detachment is seen in 30%-56% of cases [61, 63]. Strands of glial tissue extending from the

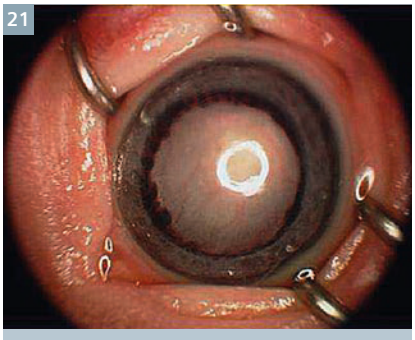

21 Elongated ciliary processes in PFV.

retina into the vitreous are seen in about one third of cases [61].

Vitreous hemorrhage from the fibrovascular tissue is common, especially in the first few months of life; hemorrhage and neovascular glaucoma are the most common complications necessitating enucleation.

The most typical finding of PFV is the retrolental fibrovascular mass [64, 68] caused by persistence of the primary vitreous that normally should regress [69].

Patients with anterior type PFV can have a good visual outcome, whilst those with posterior type tend to have a poor one [64].

Imaging findings depend on the size, thickness, and vascularity of the retrolental fibrovascular mass. At US, the main finding is a contracting echogenic retrolental mass, with one or few hyperechoic band/s extending from the mass to the optic nerve head. This band corresponds to the Cloquet canal (Fig. 22). Sometimes, the hyaloid artery can be seen within this band with Doppler US. Mafee et al. initially described the relationship between leukocoria and CT findings of a funnel-shaped mass of fibrovascular tissue that occupies the retrolental space and the site of the Cloquet canal [70], extending from the area of the optic disc toward the posterior aspect of the lens [71]. Use of CT depicts well microphthalmos and frequently a retrolental focus of increased attenuation. A linear band or septum extending from the posterior aspect of the retrolental mass allows for a confident diagnosis of PFV, such as a layering attenuating hemorrhage in the globe. CT usually demonstrates tubular, cylindrical, triangular, or discrete intravitreal densities suggesting the presence of remnants of persistent hyaloid system or congenital non-attachment of the retina. A generalized increase in intravitreal density and enhancement of abnormal intravitreal tissue are both possible [70, 71]. CT may also detect the presence of calcifications, very rare in PFV; 3D gradient echo T2-weighted MR images and SWI MR images hopefully will replace CT in the calcification depiction also in this pathology. MRI usually depicts an inconstant contrast-enhancing mass behind the lens associated to retinal and/or posterior hyaloid detachment with hemorrhage and the abnormal lens in a microophthalmic eye (Fig. 23). Visualization of a vertical septum (Cloquet canal) between the optic disc and posterior lens is a diagnostic hallmark. Decubitus positioning may also show a gravitational effect on a fluid level within the globe, reflecting a sero-hematic fluid (Fig. 24). There may also be enhancement of the anterior chamber, which is thought to be related to elongation of the ciliary processes, possibly through the mechanism of leaky vessels [64].

Anterior PFV is rarer than posterior PFV, and mixed type is by far the most frequent (Fig. 25). In the sporadic cases documented with MRI in the pertinent literature, anterior PFV showed a shallow anterior chamber, a flat lens, and an enhancement of the lens and of the ciliary body after intravenous gadolinium administration [60, 72].

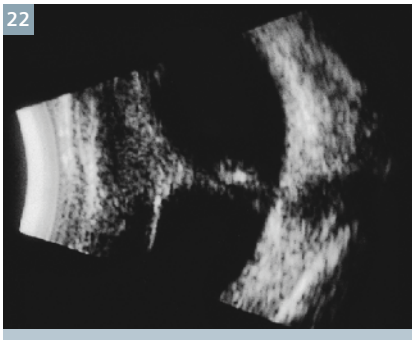

22 Retrolental stalk along the Cloquet canal.

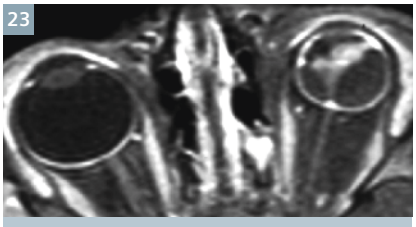

23 T1-weighted contrast-enhanced image showing retrolental mass in a microophthalmic left eye.

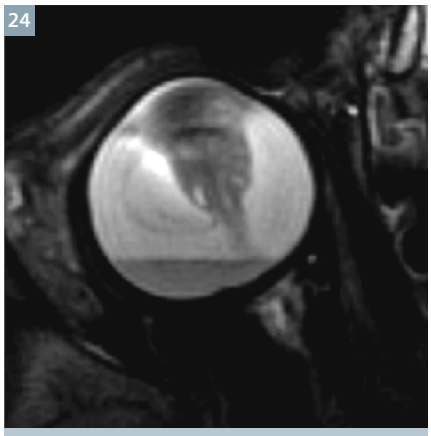

24 Fluid-fluid level due to intravitreal hemorrhage.

25 T2-weighted image of PFV with both anterior and posterior segments involvement.

Coat's disease

Since its original description in 1908, Coat's disease (CD) has been recognized as an idiopathic cause of severe vision loss with a remarkable diversity in clinical presentation and morphology. CD is a rare, probably congenital, nonfamilial, idiopathic vascular developmental disease of the retina, primarily caused by a defect at the endothelial cell level of the blood-retinal barrier, resulting in increasing amounts of yellowish intraretinal and subretinal exudate composed of blood components rich in cholesterol crystals, cholesterol- and pigment-laden macrophages, few erythrocytes, and minimal hemosiderin, final leakage of fluid into the vessel wall and perivascularly (Figs. 26, 27). The massive subretinal and intraretinal exudation often leads to thickening of the retina (heaviest in the outer sectors) and exudative retinal detachment [73, 74]. Some eyes develop retinal or choroidal neovascularization, which might result in hemorrhage. In up to 20% of all cases there is a fibrous submacular nodule that occasionally is calcified

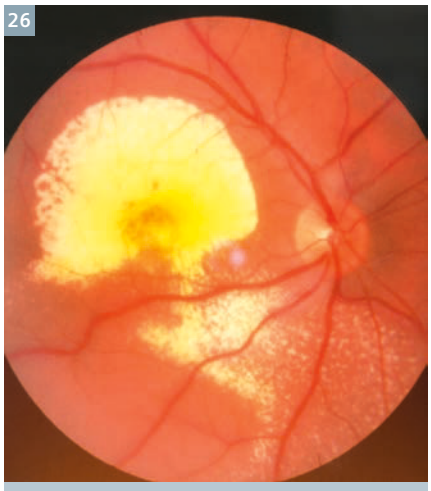

26 Yellowish exudate at ophthalmoscopy.

27 Cholesterol crystals at histology.

or ossified. The clinical spectrum of CD is broad, ranging from asymptomatic perifoveal telangiectasis, to total exudative retinal detachment with poor visual prognosis, and may progress to neovascular glaucoma with eventual phthisis bulbi. Secondary changes also include rubeosis iridis, neovascular glaucoma, cataract, and uveitis. Shields et al. [75] proposed the most recent classification system in five stages:

Stage 1: retinal teleangectasia only

Stage 2: teleangectasia and exudation

Stage 3a: exudative subtotal retinal detachment

Stage 3b: exudative total retinal detachment

Stage 4: total retinal detachment and glaucoma

Stage 5: advanced end-stage disease

The vascular anomaly of CD, although present at birth, usually does not cause symptoms until the retina detaches and central vision is lost [76, 77]. Calcifications are very rare, although intraocular bone formation has been reported in advanced cases [78]. CD is unilateral in 80%-90% of patients, affecting 69%-85% of males. If bilateral, one eye is usually minimally affected [59, 79-81].

The disease usually appears in patients slightly older (4-8 years) than those affected by RB. Several exceptions to the usual age at presentation have been reported [77, 82, 83]. CD is isolated in the majority of cases, although associations with a variety of exudative retinopathies, as well as several conditions, have been described [59, 84-87].

Leukocoria and strabismus are the most common presenting signs of CD [73, 74, 77, 79, 88-91]. Progression to total retinal detachment, painful neovascular glaucoma, phthisis bulbi, and blindness, occurs in slightly more than half of untreated patients [83, 92]. Spontaneous remission has been sporadically reported [93].

Misdiagnosing CD as RB may result in the enucleation of a potentially salvageable eye; conversely, mistaking a case of RB for CD delays the appropriate therapeutic intervention and increases the possibility of extraocular tumor spread, especially if intraocular surgery is performed.

Ophthalmoscopy can demonstrate a variety of findings, depending on the stage of the disease. In early stages, ophthalmoscopic examination reveals dilated and saccular aneurysmal changes in tortuous retinal vessels with exudates, and localized foci of retinal teleangiectasia [73]. With progression of the disease, the vascular abnormalities are associated with increasing amounts of yellow intraretinal and subretinal exudation. The ophthalmoscopic distinction of advanced CD from other diseases with bullous retinal detachment (such as RB) can be extremely difficult, if not impossible (Fig. 28); for instance, dilated retinal vessels and subretinal exudate with foamy macrophage may represent a so called 'Coat's reaction' to RB [74]. Furthermore, patients with advanced CD frequently manifest a clouded vitreous, which limits ophthalmoscopic findings. Fluorescein angiography plays a pivotal role in both diagnosis and assessment of disease progression, allowing clear visualization of the vascular changes which may be taking place [75]. It may show mildly irregular retinal vessels, sausage-like vascular beading, saccular outpouchings, or light-bulb dilations; leakage from the irregular-caliper retinal vessels may be demonstrated (Fig. 29).

The ultrasonographic findings depend on the stage of the disease. In the early stages, US shows areas of retinal detachment, and excludes the presence of solid mass and calcification (both suggesting RB); documentation of teleangiectasia and retinal exudates are also possible in early stages. When the disease advances, some more characteristic echographic signs may help the right diagnosis: narrow or close V-shaped retinal detachment with looping of a thickened peripheral retina, poor retinal mobility, dense slowly moving

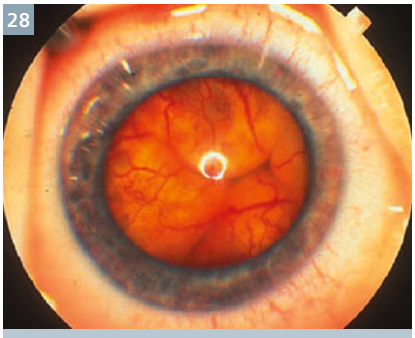

28 Bullous retinal detachment in Coat's disease.

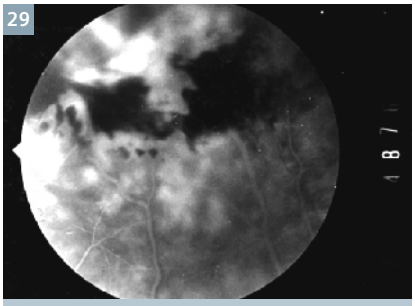

29 Leakage at fluorangiography.

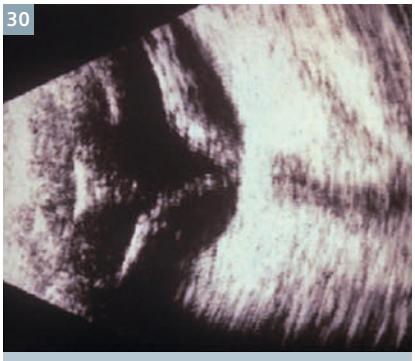

30 Funnel-shaped total retinal detachment at ultrasonography.

subretinal opacities, as well as the above described absence of solid mass and no evidence of calcification (Fig. 30). However, it is important to remember that looping of the peripheral retina may also be seen in advanced retinopathy of prematurity (ROP), and calcification has been described in longstanding CD [95]. Unfortunately, although ultrasonography is an essential component of the evaluation of patients with CD, it is of limited utility when diffuse vitreous infiltration, non-calcified masses, and complex interfaces are present. OCT is useful in identifying subtle macular edema or cystic changes, subretinal fluid, exudate, and hemorrhage, as well as assessment of the integrity of specific retinal layers [96].

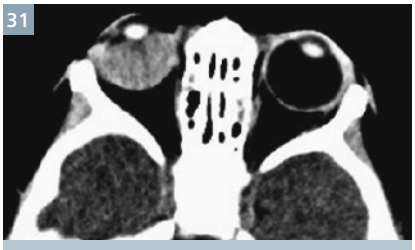

31 CT scan showing diffuse hyperdensity in the right eye in high-grade Coat's disease. No calcifications are visible.

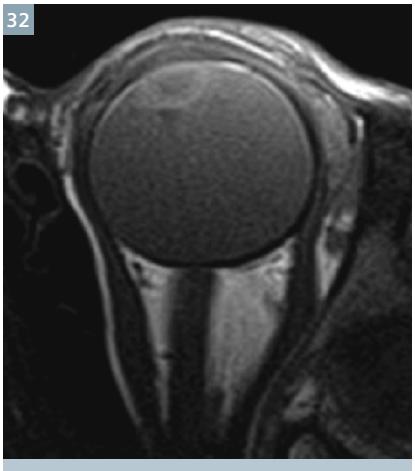

32 T1-weighted not-enhanced image showing diffuse hyperintense exudate in the affected eye.

When clinical diagnosis is uncertain, CT and/or MR imaging are required. In the initial stages, imaging studies may be essentially normal or show very slight focal retinal thickening and exudate. In advanced stages, CT and MRI show a funnel-shaped retinal detachment with an underlying subretinal lipo-proteinaceous exudation. The exudate may occupy almost the entire globe and may obliterate the vitreous space in advanced cases. There is no calcification. The exudation appears hyperdense on CT (Fig. 31) and almost always as hyperintense signal on both T1w (Fig. 32), T2w (Fig. 33), and FLAIR (Fig. 34) images. This is in contrast

33 T2-weighted image showing hyperintense exudate and totally detached retina with some peripheral thickening.

34 FLAIR image clearly showing a hyperintense right eye.

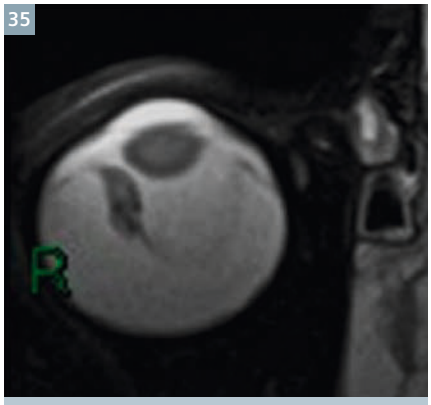

35 T2-weighted image showing a hypointense mass-like lesion in Coat's disease.

to RB, which is relatively hypointense on T2-weighted images. The presence of hemorrhage at different catabolic stages or fibrosis may confer a potentially confounding heterogeneous appearance, especially on T2-weighted images (Fig. 35). Post-contrast study usually shows an absence of enhancement in the subretinal region, and may document characteristic funnel-shaped enhancement of the detached leaves of the retina (Fig. 36), due to thickened retina with teleangectasia and microaneurysms, especially in the peripheral sections. Enhancement of the detached leaves of the retina, if present, may be very important in the differential diagnosis with RB, which enhances in a mass-like fashion. However, in extreme cases of advanced CD, a retrolental gliotic mass can occur simulating nodular RB.

A case report with enhancement of the proximal optic nerve in T1-weighted contrast-enhanced images has been described in a child with elevated (58 mm Hg) intraocular pressure (IOP); the finding disappeared after normalization of IOP [97].

Proton MR spectroscopy of the exudate has demonstrated a peak at 1-1.6 ppm due to lipoproteinaceous material [98].

The main problem in differential diagnosis remains to differentiate advanced CD from RB, and usually requires the summation of various diagnosis aids, since both diseases may present with nonrhegmatogenous retinal detachment, teleangiectases, and subretinal collections.

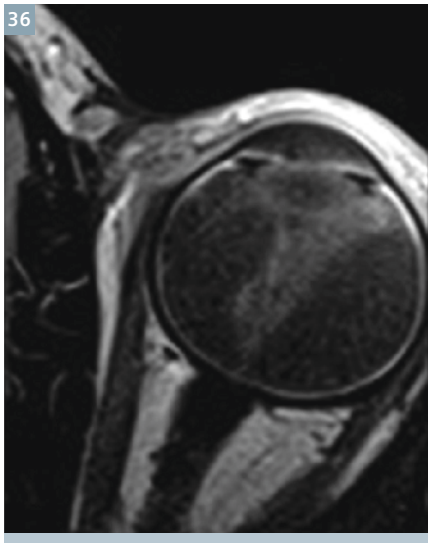

36 T1-weighted contrast-enhanced image showing enhancement of thickened detached retina.

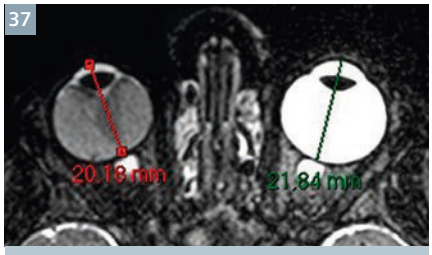

37 T2-weighted image showing the smaller diameter of the affected eye in Coat's disease.

Exceptions to the typical imaging features are seen in both CD and RB [73, 77, 99, 100]. Particularly, a retrolental contrast-enhancing gliotic mass simulating nodular RB can occur in extreme cases of advanced Coat's disease [101]. The rare DIRB may not show nodularity on any imaging studies [102]. DIRB may also simulate CD due to the diffuse pattern, rare presence of calcification and lack of underlying mass [2].

Furthermore, occasional reports of calcifications in CD have been well documented [73, 76, 99, 100]. In the chronic stages of CD, the MR signal intensity of subretinal fluid may become heterogeneous due to the combination of cholesterol crystals, hemorrhage in different stages of hemoglobin catabolism, PAS-positive material, and scarring [59, 77, 101], resulting in signal intensities which differ from the typical pattern.

A significantly smaller volume of the affected globe, always noted in CD, is an additional clue in the differential diagnosis with RB [82]; retinal vascular developmental abnormalities of CD may disturb the release of growth factors regulating the further development of secondary vitreous, and thus resulting in the disturbance of the growth of the affected globe (Fig. 37).

References

1 De Potter P, Flanders AE, Shields JA et Al: The role of fat-suppression technique and gadopentetate dimeglumine in magnetic resonance imaging evaluation of intraocular tumors and simulating lesions. Arch Ophthal- mol 112: 340-348, 1994.

2 Smirniotopoulos JG, Bargallo N, Mafee MF: Differential diagnosis of leuko- coria: radiologic-pathologic correlation. Radiographics 14: 1059-1079, 1994.

3 De Potter P, Shields JA, Shields CL: Tumors and pseudotumors of the retina. In: De Potter P, Shields JA, Shields CL (eds.). MRI of the eye and oRBit. Philadelphia: JB Lippincott Company 1995: 93-116.

4 Shields CL, Schoenberg E, Kocher K, Shukla SY, Kaliki S, Shields JA. Lesions simulating retinoblastoma (pseudoreti- noblastoma) in 604 cases: results based on age at presentation. Ophthal- mology. 2013;120(2):311-6.

5 Balmer A, Munier F. Differential diagnosis of leukocoria and strabismus, first presenting signs of retino- blastoma. Clin Ophthalmol. 2007;1(4):431-9.

6 Apushkin MA1, Apushkin MA, Shapiro MJ, Mafee MF. Retinoblastoma and simulating lesions: role of imaging. Neuroimaging Clin N Am. 2005 Feb;15(1):49-67.

7 Rao AA, Naheedy JH, Chen JY, Robbins SL, Ramkumar HL. A clinical update and radiologic review of pediatric oRBital and ocular tumors. J Oncol. 2013;2013:975908. doi: 10.1155/2013/975908. Epub 2013 Mar 12.

8 Schueler AO, Hosten N, Bechrakis NE, Lemke AJ, Foerster P, Felix R, Foerster MH, Bornfeld N.. High resolution magnetic resonance imaging of retino- blastoma. Br J Ophthalmol 2003 Mar;87(3):330-5.

9 Shields CL, Shields JA. Diagnosis and management of retinoblastoma. Cancer Control. 2004;11:317–327.

10 Kivela T. Trilateral retinoblastoma: a meta-analysis of hereditary retino- blastoma associated with primary ectopic intracranial retinoblastoma. J Clin Oncol. 1999;17:1829–1837.

11 Singh AD, Shields CL, Shields JA: Prognostic factors in retinoblastoma. J Pediatr Ophthalmol Strabismus 37: 134-141, 2000.

12 Finelli DA, Shurin SB, Bardenstein DS: Trilateral Retinoblastoma: Two Variations. Am J Neuroradiol 16: 166-170, 1995.

13 Provenzale JM, Weber AL, Klintworth GK et Al: Bilat- eral retinoblastoma with coexistent pinealoblastoma (trilateral retinoblastoma). Radiologic-pathologic corre- lation. Am J Neuroradiol 16: 157-165, 1995.

14 Reese A, Ellsworth R. Evaluation and current concept of retinoblastoma theraphy. Trans Am Acad Ophthalmolo Otorlaryngol 1963; 67: 164-172.

15 Murphree AL Intraocular retinoblastoma: the case for a new group classification. Ophthalmol Clin N Am 2005; 18: 41–53.

16 Shields CL, Ghassemi F, Tuncer S, Thangappan A, Shields JA. Clinical spectrum of diffuse infiltrating retino- blastoma in 34 consecutive eyes. Ophthalmology. 2008;115(12):2253-8.

17 Vasquez LM1, Giuliari GP, Halliday W, Pavlin CJ, Gallie BL, Héon E. Ultrasound biomicroscopy in the management of retinoblastoma. Eye 2011; 25: 141-147.

18 Mahajan A, Crum A, Johnson MH, Materin MA. Ocular neoplastic disease. Semin Ultrasound CT MR. 2011;32(1):28-37.

19 Rauschecker AM, Patel CV, Yeom KW, Eisenhut CA, Gawande RS, O'Brien JM, Ebrahimi KB, Daldrup-Link HE. High- resolution MR imaging of the oRBit in patients with retinoblastoma. Radio- graphics. 2012;32(5):1307-26.

20 Roth DB, Scott IU, Murray TG et Al: Echography of retinoblastoma: histo- pathologic correlation and serial evalu- ation after globe-conserving radio- therapy or chemotherapy. J Pediatr Ophthalmol Strabismus 38: 136-143, 2001.

21 Razek AA, Elkhamary S. MRI of retino- blastoma. Br J Radiol. 2011;84(1005):775-84.

22 Kaufman LM, Mafee MF, Song CD: Retinoblastoma and simulating lesions. Radiol Clin North Am 36: 1101- 1117, 1998.

23 Finger PT, Harbour W, Karcioglu Z. Risk factors for metastasis of retinoblastoma. Surv Ophthalmol 2002;47:1–36.

24 Shields CL1, Materin MA, Shields JA. Review of optical coherence tomography for intraocular tumors. Curr Opin Ophthalmol. 2005 Jun;16(3):141-54.

25 Villegas VM1, Hess DJ, Wildner A, Gold AS, Murray TG. Retinoblastoma. Curr Opin Ophthalmol. 2013;24(6):581-8.

26 Yousef YA, Schroff M, Halliday W, Gallie BL, Héon E. Detection of optic nerve disease in retinoblastoma by use of

spectral domain optical coherence tomography. J AAPOS 2012; 16: 481-483.
27 de Graaf P, Göricke S, Rodjan F, Galluzzi P, Maeder P, Castelijns JA, Brisse HJ; European Retinoblastoma Imaging Collaboration (ERIC). Guidelines for imaging retinoblastoma: imaging principles and MRI standardization. Pediatr Radiol. 2012 Jan;42(1):2-14.
28 Brennan RC, Wilson MW, Kaste S, Helton KJ, McCarville MB. US and MRI of pediatric ocular masses with histopathological correlation. Pediatr Radiol. 2012;42(6):738-49.
29 Tuncer S, Oray M, Yildirim Y, Camcioglu Y, Tugal-Tutkun I. Bilateral intraocular calcification in necrotizing cytomegalovirus retinitis. Int Ophthalmol (2014) 34:1119–1122.
30 Galluzzi P, Hadjistilianou T, Cerase A, et al. Is CT still useful in the study protocol of retinoblastoma? AJNR Am J Neuroradiol. 2009;30:1760–1765.
31 Rodjan F, de Graaf P, van der Valk P, Hadjistilianou T, Cerase A, Toti P, de Jong MC, Moll AC, Castelijns JA, Galluzzi P; on behalf of the European Retinoblastoma Imaging Collaboration. Detection of Calcifications in Retinoblastoma Using Gradient-Echo MR Imaging Sequences: Comparative Study between In Vivo MR Imaging and Ex Vivo High-Resolution CT. AJNR Am J Neuroradiol. 2015 Feb;36(2):355-60.
32 Brisse HJ, Lumbroso L, Fréneaux PC, Validire P, Doz FP, Quintana EJ, Berges O,Desjardins LC, Neuenschwander SG. Sonographic, CT, and MR imaging findings in diffuse infiltrative retinoblastoma: report of two cases with histologic comparison. AJNR Am J Neuroradiol. 2001 Mar;22(3):499-504.
33 Bhatnagar R, Vine AK: Diffuse Infiltrating Retinoblas- toma. Ophthalmology 98: 1657-1661, 1991.
34 Mansour AM, Greenwald MJ, O'Grady R: Diffuse Infil- trating Retinoblastoma. J Ped Ophthalmol Strabismus 36: 152-54, 1989.
35 Shields CL, Fulco EM, Arias JD, Alarcon C, Pellegrini M, Rishi P, Kaliki S, Bianciotto CG, Shields JA. Retinoblastoma frontiers with intravenous, intra-arterial, periocular, and intravitreal chemotherapy. Eye (Lond). 2013;27(2):253-64.
36 Abramson DH, Gobin YP, Marr BP, Dunkel IJ, Brodie SE. Intra-arterial chemotherapy for retinoblastoma. Ophthalmology. 2012;119(8):1720-1; author reply 1721.
37 Venturi C, Bracco S, Cerase A, Cioni S, Galluzzi P, Gennari P, Vallone IM, Tinturini R, Vittori C, De Francesco S, Caini M, D'Ambrosio A, Toti P, Renieri A,Hadjistilianou T. Superselective ophthalmic artery infusion of melphalan for intraocular retinoblastoma: preliminary results from 140 treatments. Acta Ophthalmol. 2013;91(4):335-42.
38 Bracco S, Leonini S, De Francesco S, Cioni S, Gennari P, Vallone IM, Piu P, Galimberti D, Romano DG, Caini M, De Luca M, Toti P, Galluzzi P, Hadjistilianou T, Cerase A. Intra-arterial chemotherapy with melphalan for intraocular retinoblastoma. Br J Ophthalmol. 2013;97(9):1219-21.
39 de Graaf P, Knol DL, Moll AC, Imhof SM, Schouten-van Meeteren AY, Castelijns JA. Eye size in retinoblastoma: MR imaging measurements in normal and affected eyes. Radiology. 2007;244(1):273-80.
40 de Graaf P, Barkhof F, Moll AC, et al. Retinoblastoma: MR imaging parameters in detection of tumor extent. Radiology. 2005;235:197–207.
41 de Graaf P, Moll AC, Imhof SM, van der Valk P, Castelijns JA. Retinoblastoma and optic nerve enhancement on MRI: not always extraocular tumour extension. Br JOphthalmol. 2006;90(6):800-1.
42 Brisse HJ, Guesmi M, Aerts I, et al. Relevance of CT and MRI in retinoblastoma for the diagnosis of postlaminar invasion with normal-size optic nerve: a retrospective study of 150 patients with histological comparison. Pediatr Radiol. 2007;37:649–656.
43 Lemke AJ, Kazi I, Mergner U et al (2007) Retinoblastoma-MR appearance using a surface coil in comparison with histopathological results. Eur Radiol 17:49–60.
44 Ainbinder DJ, Haik BG, Frei DF, Gupta KL, Mafee MF (1996) Gadolinium enhancement: improved MRI detection of retinoblastoma extension into the optic nerve. Neuroradiology 38:778–781.
45 de Jong MC, de Graaf P, Noij DP, Göricke S, Maeder P, Galluzzi P, Brisse HJ, Moll AC, Castelijns JA; European Retinoblastoma Imaging Collaboration (ERIC). Diagnostic performance of magnetic resonance imaging and computed tomography for advanced retinoblastoma: a systematic review and meta-analysis. Ophthalmology 2014 ;121(5):1109-18.
46 Wilson MW, Rodriguez-Galindo C, Billups C, Haik BG, Laningham, F, Patay Z (2009) Lack of correlation between the histologic and magnetic resonance imaging results of optic nerve involvement in eyes primarily enucleated for retinoblastoma. Ophthalmology 116: 1558–1563.
47 Song KD, Eo H, Kim JH, Yoo SY, Jeon TY (2012) Can preoperative MR imaging predict optic nerve invasion of retinoblastoma? Eur J Radiol 81:4041–4045.
48 Lee BJ, Kim JH, Kim DH, Park SH, Yu YS (2012) The validity of routine brain MRI in detecting post-laminar optic nerve involvement in retinoblastoma. Br J Ophthalmol 96:1237–1241.
49 Chawla B, Sharma S, Sen S et al (2012) Correlation between clinical features, magnetic resonance imaging, and histopathologic findings in retinoblastoma: a prospective study. Ophthalmology 119:850–856.
50 Brisse HJ, de Graaf P, Galluzzi P, Cosker K, Maeder P, Göricke S, Rodjan F, de Jong MC, Savignoni A, Aerts I, Desjardins L, Moll AC, Hadjistilianou T, Toti P, van der Valk P, Castelijns JA, Sastre-Garau X; on behalf of the European Retinoblastoma Imaging Collaboration (ERIC). Assessment of early-stage optic nerve invasion in retinoblastoma using high-resolution 1.5 Tesla MRI with surface coils: a multicentre, prospective accuracy study with histopathological correlation. Eur Radiol. 2014 Nov 30.
51 Galluzzi P, Cerase A, Hadjistilianou T, De Francesco S, Toti P, Vallone IM, Filosomi G, Monti L, Bracco S, Gennari P, Ginanneschi C, Venturi C. Retinoblastoma: Abnormal gadolinium enhancement of anterior segment of eyes at MR imaging with clinical and histopathologic correlation. Radiology. 2003;228(3):683-90.
52 de Graaf P, van der Valk P, Moll AC, Imhof SM, Schouten-van Meeteren AY, Knol DL, Castelijns JA. Contrast-enhancement of the anterior eye segment in patients with retinoblastoma: correlation between clinical, MR imaging, and histopathologic findings. AJNR Am J Neuroradiol. 2010;31(2):237-45.
53 de Graaf P, Pouwels PJ, Rodjan F, Moll AC, Imhof SM, Knol DL, Sanchez E, van der Valk P, Castelijns JA. Single-shot turbo spin-echo diffusion-weighted imaging for retinoblastoma: initial experience. AJNR Am J Neuroradiol. 2012;33(1):110-8.
54 Sepahdari AR, Kapur R, Aakalu VK, Villablanca JP, Mafee MF. Diffusion-weighted imaging of malignant ocular masses: initial results and directions for further study. AJNR Am J Neuroradiol. 2012;33(2):314-9.
55 Abdel Razek AA, Elkhamary S, Al-Mesfer S, Alkatan HM. Correlation of apparent diffusion coefficient at 3T with prognostic parameters of retinoblastoma. AJNR Am J Neuroradiol. 2012;33(5):944-8.
56 Rodjan F, de Graaf P, van der Valk P, Moll AC, Kuijer JP, Knol DL, Castelijns JA, Pouwels PJ. Retinoblastoma: value of dynamic contrast-enhanced MR imaging and correlation with tumor angiogenesis. AJNR Am J Neuroradiol. 2012;33(11):2129-35.
57 Rodjan F, Graaf P, Moll AC, et al. Brain abnormalities on MR imaging in patients with retinoblastoma. AJNR Am J Neuroradiol. 2010;31:1385–1389.
58 Rodjan F, de Graaf P, Brisse HJ, Göricke S, Maeder P, Galluzzi P, Aerts I, Alapetite C, Desjardins L, Wieland R, Popovic MB, Diezi M, Munier FL, Hadjistilianou T, Knol DL, Moll AC, Castelijns JA. Trilateral retinoblastoma: neuroimaging characteristics and value of routine brain screening on admission. J Neurooncol. 2012;109(3):535-44.

59 Edward DP, Mafee MF, Garcia-Valenzuela E, Weiss RA. Coats' disease and persistent hyperplastic primary vitreous—role of MR imaging and CT. Radiol Clin North Am 1998; 36 (6) 1119-1131.
60 Castillo M, Wallace DK, Mukherji SK. Persistent hyperplastic primary vitreous involving the anterior eye. AJNR Am J Neuroradiol 1997;18(8):1526–15281998; 36(6):1119–1131.
61 Haddad R, Font RL, Reeser F. Persistent hyperplastic primary vitreous: a clinico-pathologic study of 62 cases and review of the literature. Surv Ophthalmol 1978;23(2):123–134.
62 Reese AB. Persistent hyperplastic primary vitreous. Trans Am Acad Ophthalmol Otolaryngol 1955;59(3):271–295.
63 Pollard ZF. Persistent hyperplastic primary vitreous: diagnosis, treatment and results. Trans Am Ophthalmol Soc 1997;95:487–549.
64 Kumar A, Jethani J, Shetty S, Vijayalakshmi P. Bilateral persistent fetal vasculature: a study of 11 cases. J AAPOS 2010;14(4): 345–348.
65 Jain TO. Bilateral persistent hyperplastic primary vitreous. Indian J Ophthalmol 2009; 57:53-54.
66 Galal AH, Kotoury AIS, Azzab AA. Bilateral persistent hyperplastic primary vitreous: An Egyptian family supporting a rare autosomal dominant heritance. Genet Couns 2006; 17: 441-447.
67 Sanghvi DA, Sanghvi CA, Purandare NC. Bilateral persistent hyperplastic primary vitreous. Australas Radiol 2005; 49: 72-74.
68 Pediatric Orbit Tumors and Tumorlike Lesions: Neuroepithelial Lesions of the Ocular Globe and Optic Nerve. Chung EM, Specht CS, Schroeder JW. Radiographics 2007; 27 (4):1159-1187.
69 Shastry BS. Persistent hyperplastic primary vitreous: congenital malformation of the eye. Clin Experiment Ophthalmol 2009;37(9): 884–890.
70 Goldberg MF, Mafee MF. Computed tomography for diagnosis of persistent hyperplastic primary vitreous (PHPV). Ophthalmology 1983. 90 (5) :442-451.
71 Mafee MF, Goldberg MF. Persistent hyperplastic primary vitreous (PHPV): role ot computed tomography and magnetic resonance. Radiol Clin North Am.1987 25 (4): 683-692.
72 Sun MH, Kao LY, Kuo YH. Persistent hyperplastic primary vitreous: magnetic resonance imaging and clinical findings. Chang Gung Med J. 2003;26(4):269-76.
73 Chang M, Mc Lean IW, Merritt JC: Coat's disease: a study of 62 histologically confirmed cases. J Pediatr Ophthalmol Strabismus 21: 163-168, 1984.
74 Kremer I, Nissehorn I, Ben-Sira I: Cytologic and biochemical examination of the subretinal fluid in the diagnosis of Coat's disease. Acta Ophthalmol (Copenh) 1989; 67: 342- 346.
75 Shields JA, Shields CL, Honavar SG, Demirci H, Cater J: Classification and management of Coats disease: the 2000 Proctor Lecture. Am J Ophthalmol 2001;131:572–583.
76 Mafee MF: Imaging of the globe. In: Valvassori GE, Mafee MF, Carter BL. Imaging of head and neck. Thieme: 216-246, 1995.
77 Haik BG: Advanced Coat's disease. Tr Am Ophth Soc 89: 371-475, 1991.
78 Steidl SM, Hirose T, Sang D t Al: Difficulties in exclud- ing the diagnosis of retinoblastoma in cases of advanced Coat's disease; a clinicopathologic report. Ophthalmo- logica 210: 336-340, 1996.
79 Woods AC, Duke JR. Coats's disease. I. Review of the literature, diagnostic criteria, clinical findings, and plasma lipid studies. Br J Ophthalmol 1963;47:385–412.
80 Shields JA, Shields CL. Review: Coats disease—the 2001 LuEsther T. Mertz lecture. Retina 2002;22(1):80–91.
81 Egerer I, Tasman W, Tomer TT. Coats disease. Arch Ophthalmol 1974;92(2):109–112.
82 Galluzzi P, Venturi C, Cerase A et al: Coat's disease: smaller volume of the affected globe. Radiology 221: 64- 69, 2001.
83 Kirath H, Eldem B. Management of moderate to ad- vanced Coat's disease. Ophthalmologica 212: 19-22, 1998.
84 Solomon A, Banin E, Anteby I et al: Retinitis pigmen-tosa, Coat's disease and uveitis. European Journal of Ophthalmology 9: 202-205, 1999.
85 Park DH, Kim IT. Patient with Parry-Romberg syndrome complicated by Coats' syndrome Jpn J Ophthalmol. 2008 ; 52(6):520-2.
86 Crow YJ, McMenamin J, Haenggeli CA, Hadley DM, Tirupathi S, Treacy EP, Zuberi SM, Browne BH, Tolmie JL, Stephenson JB. Coats' plus: a progressive familial syndrome of bilateral Coats' disease, characteristic cerebral calcification, leukoencephalopathy, slow pre- and post-natal linear growth and defects of bone-marrow and integument Neuropediatrics 2004, 35(1); 10-19.
87 Romaniello R1, Arrigoni F, Citterio A, Tonelli A, Sforzini C, Rizzari C, Pessina M, Triulzi F, Bassi MT, Borgatti R. Cerebroretinal microangiopathy with calcifications and cysts associated with CTC1 and NDP mutations. J Child Neurol. 2013,28(12):1702-8.
88 Coats G: Forms of retinal disease with massive exudation. R Lond Ophthalmol Hosp Res 17: 440-525, 1908.
89 Gomez Morales A: Coat's disease: natural history and results of treatment. Am J Ophthalmol 60: 855-865, 1965.
90 Tripathi R, Ashton N: Electron microscopical study of Coat's disease. Br J Ophthalmol 55: 289-301, 1971.
91 Spitznas M, Joussen F, Wessing A et Al: Coat's disease. An epidemiologic and fluorescein angiographic study. Albrecht Graefes Arch Klin Ophthalmol 195: 241-250, 1975.
92 Char DH: Coat's syndrome: long term follow up. Br J Ophthalmol 84: 37-39, 2000.
93 Deutsch TA, Rabb MF, Jampol LM: Spontaneous regression of retinal lesions in Coat's disease. Can J Ophthalmol 17: 169-172, 1982.
94 Jaffe MS, Shields JA, Canny CL et Al: Retinoblastoma simulating Coat's disease: a clinicopathologic report. Ann Ophthalmol 9: 863-868, 1977.
95 Atta HR, Watson N: Echographic Diagnosis of Advanced Coat's Disease. Eye 6: 80-85, 1992.
96 Sigler EJ, Randolph JC, Calzada JI, Wilson MW, Haik BG. Current management of Coats disease. Surv Ophthalmol. 2014;59(1):30-46.
97 Dhoot DS, Weissman LJ, Landon RE, Evans M, Stout T. Optic nerve enhancement in Coats disease with secondary glaucoma. Journal of AAPOS. 2009; 13 (3): 301-302.
98 Eisenberg L, Castillo M, Kwock L, Mukherji SK, Wallace DK. Proton MR spectroscopy in Coats disease. AJNR Am J Neuroradiol 1997;18(4):727–729.
99 Senft SH, Hidayat AA, Cavender JC: Atypical presentation of Coat's disease. Retina 14: 36-38, 1994.
100 Pe'er J: Calcifications in Coat's disease. Am J Ophthalmol 106: 742-743, 1988.
101 Shields JA, Shields CL: Intraocular tumors: a text and atlas. Philadelphia, Saunders vol 341, pp. 356-359, 1992.
102 Villablanca JP, Mafee MF, Kaufman LM et Al: Facies to remember. Retinoblastoma, Coat's disease, and toxocariasis. Int J Neuroradiol 4: 41-50, 1998.

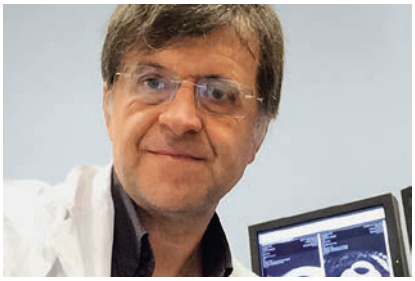

Contact

Paolo Galluzzi
Neuroimaging and Neuro-interventional Unit (NINT)
Azienda Ospedaliera e Universitaria Senese
Siena
Italy
galluzzip@libero.it